Modular Filter-based Approach to Ground Motion Attenuation Modeling

Vladimir Graizer[1] and Erol Kalkan[2]

INTRODUCTION

Previous-generation ground-motion attenuation relations (*e.g.*, Abrahamson and Silva 1997; Boore *et al.* 1997; Campbell 1997; Sadigh *et al.* 1997) were designed to predict ground motion at distances less than 100 km from an earthquake fault. As probabilistic and deterministic seismic hazard analysis concepts have become more prevalent in performance-based seismic design, these relations have been used in practice much beyond their distance limitation. Realizing the engineering needs for predicting ground motions at distances farther than 100 km, the Next Generation Attenuation (NGA) relations project targeted a distance range up to 200 km (Power *et al.* 2006). For seismic hazard analysis in the western United States (WUS), 200 km is a sufficiently large distance to quantify design-basis hazard level from known active faults due to relatively fast attenuation of ground motion. For the central and eastern United States (CEUS), ground motion attenuates more slowly, yet design of critical infrastructures in the CEUS (*e.g.*, nuclear power plants) requires computation of seismic hazard from distant large events. Thus, the recently initiated NGA-East project for CEUS set a goal to design ground-motion attenuation models applicable to 1,000 km. The objective of this article is to revisit the commonly used empirical approach to ground-motion attenuation modeling and compare it with an alternative modular filter-based approach that can be effectively used for predicting ground motion at near- (<10 km), intermediate- (~10 km to 100 km), and far-field distances (>100 km). In this latter approach, each filter is calibrated separately to represent a certain physical phenomenon affecting seismic radiation from the source. We demonstrate that the modular filter-based approach provides accurate (that is, expected median prediction without significant bias) and efficient (that is, relatively small standard error of prediction) predictions. We also present our peak ground acceleration (PGA) based predictive model for 5% damped spectral acceleration (SA) ordinates as a continuous function of period.

1 U.S Nuclear Regulatory Commission
2 U.S. Geological Survey

BRIEF HISTORY OF MATHEMATICAL REPRESENTATION OF GROUND-MOTION ATTENUATION

A general ground-motion (GM) prediction equation is:

$$GM = f(M, R, C) \tag{1}$$

where M is a moment magnitude (local magnitude in earlier studies), R is a closest distance to the fault (epicentral distance in earlier studies, or Joyner-Boore (R_{JB}) distance), and C is a set of independent parameters representing style of faulting, shallow site, deep sediment (that is, basin), directivity, and other physical effects.

Strong ground-motion attenuation relations in seismology date back to the 1960s (Esteva and Rosenblueth 1964). A summary of attenuation relations developed since then is given in Douglas (2001, 2002). As was stated by Bolt and Abrahamson (1982), the first critical step in modeling is the selection of an approximation function that best fits ground-motion attenuation with distance. Up until the mid 1980s, different approaches and approximation formulas were explored (*e.g.*, Milne and Davenport 1969; Esteva 1970; Schnabel and Seed 1973; Donovan 1973; Ambraseys 1975; Trifunac and Brady 1975; Campbell 1981; Joyner and Boore 1981). To model ground-motion attenuation with distance, Milne and Davenport (1969) used the following formula:

$$GM = \frac{a_1 \exp(a_2 M)}{a_3 \exp(a_4 M) + R^2} \tag{2}$$

where $a_{1....4}$ are the estimator coefficients. Esteva (1970) used a similar formula with the same distance decay (that is, R^{-2}). Donovan (1973) and later Campbell (1981) used a similar type of relation with a slower decay:

$$GM = \frac{a_1 \exp(a_2 M)}{[R + C(M)]^n} \text{ with } 1.09 < n < 1.75. \tag{3}$$

doi: 10.1785/gssrl.82.1.21

Schnabel and Seed (1973) suggested the following attenuation formulation:

$$GM = {a_1}/{R^n} \quad \text{with } 1.5 < n < 2.0. \tag{4}$$

Equations 2–4 represent ground-motion attenuation as a power-law with slope n ranging from 1 to 2. Trifunac and Brady (1975) and Trifunac (1976) suggested a different expression:

$$\log_{10}(GM) = M + \log_{10} A_0(R) - \log_{10} a_0(M) \tag{5}$$

where $\log_{10} A_0(R)$ is an empirically determined attenuation function used for calculation of local magnitude M_L, and $\log_{10} a_0(M)$ is a magnitude scaling function. Ambraseys (1975) also suggested a logarithmic type of dependency:

$$\ln(GM) = a_1 + a_2 M_L + a_3 \ln R\,. \tag{6}$$

The expressions from Trifunac and Brady (1975) and Ambraseys (1975) seem to be the first of their kind to use a logarithmic type of relation for peak ground-motion attenuation modeling. Later, Joyner and Boore (1981) combined geometrical spreading with anelastic attenuation:

$$\ln(GM) = a_1 + a_2 M + a_3 \ln R + a_4 R\,. \tag{7}$$

Since the late 1980s, approximations similar to Equation 7 have been commonly used in attenuation relations (*e.g.*, Abrahamson and Silva 1997; Campbell 1997; Sadigh *et al.* 1997; Boore *et al.* 1997). According to Campbell (2003), an attenuation relation in its most fundamental form can be expressed as:

$$\ln(GM) = a_1 + a_2 M - a_3 \ln R + a_4 R + a_5 F + a_6 S + \sigma \tag{8}$$

where F is a parameter characterizing the style of faulting, S is a parameter characterizing site condition, and σ is a random error term with zero mean (normally distributed). Most current attenuation relation developers follow the modeling approach based on Equation 8 (*e.g.*, Abrahamson and Silva 2008; Boore and Atkinson 2008; Campbell and Bozorgnia 2008; Chiou and Youngs 2008; Idriss 2008). Since ground-motion data is considered to be log-normally distributed, the transition from linear (Equation 1) to logarithmic (Equation 8) domain simplifies data fitting by linearization in regression. On the other hand, it pushes researchers to search for a fixed functional form between logarithm of ground-motion intensity measure and magnitude, distance, and other independent parameters appropriate for both near- and far-field. This practice generally results in complex dependencies between dependent and independent parameters.

ATTENUATION CHARACTERISTICS OF PGA AND ITS MODELING

According to the wave propagation theory, in an elastic homogeneous medium residual displacements from a point source attenuate as R^{-2}, P and S waves attenuate as R^{-1}, and surface waves attenuate as $R^{-0.5}$ (Chinnery 1961; Haskell 1969). This means that ground-motion attenuation theoretically follows a power law and its order changes from near- to far-field. The actual attenuation is much more complex because an earthquake source is not a point, and anelastic and scattering effects also take place in heterogeneous media. To see how recorded ground motion attenuates in the near-field, consider the spatial distribution of ground-motion data recorded in the proximity of earthquake fault zones (*e.g.*, Mogul 2008 [Nevada]; Parkfield 2004 [California]; Chi-Chi 1999 [Taiwan]; and Northridge 1994, Loma Prieta 1989, and Imperial Valley 1979 [California]). These reveal the following important attenuation characteristics of PGA:

1. remains constant in near-field (flat response—no attenuation),
2. exhibits an increase in amplitude (bump on attenuation curve) or a turning point (that is, decay) at certain distances (about 3–10 km from the fault rupture),
3. attenuates as R^{-1} and faster at distances greater than 10 km,
4. its amplitude amplifies at certain distances due to basin effect or reflection from the Moho surface, and
5. depending upon crustal characteristics, it can attenuate much faster at distances larger than 100 km due to regional low Q values, as it is the case in the WUS.

As shown in Figure 1A, the 2004 **M** 6.0 Parkfield earthquake is a well-recorded event at both near- and far-field. Figure 1B shows PGA data for the 1979 **M** 6.5 Imperial Valley earthquake. The attenuation characteristic of the Parkfield and Imperial Valley earthquakes is similar to that from a frequency response function of a single degree of freedom (SDF) oscillator: flat response at low frequencies, a bump and a turning point, and sharp decay. The frequency response function of an SDF oscillator can be expressed as:

$$G(\lambda) = {A}/{\sqrt{(1-\lambda^2)^2 + 4D_0^2\lambda^2}} \tag{9}$$

where $\lambda = \omega/\omega_0$, and A is the amplification coefficient (that is, scaling parameter), ω is the cyclic frequency, ω_0 is the natural cyclic frequency, and D_0 is a damping term. Substituting the square of frequency (ω^2) term with the distance (R) term, we obtain the core attenuation equation as first introduced in Graizer and Kalkan (2007):

$$G\ (M,R,C_0) = {1}/{\sqrt{\left[1-(R/R_0)\right]^2 + 4D_0^2(R\ \ /R_0)}}\,. \tag{10}$$

In Equation10, R_0 is the corner distance, which is directly proportional to the magnitude of the earthquake. The larger the earthquake, the wider the area with no attenuation of peak parameters. Data show that R_0 varies from 4 km for **M** 5 to about 10 km for **M** 8 (Graizer and Kalkan 2007). A certain analogy can also be seen between the R_0 and the corner frequency in Brune's model (1970, 1971) since both are related to

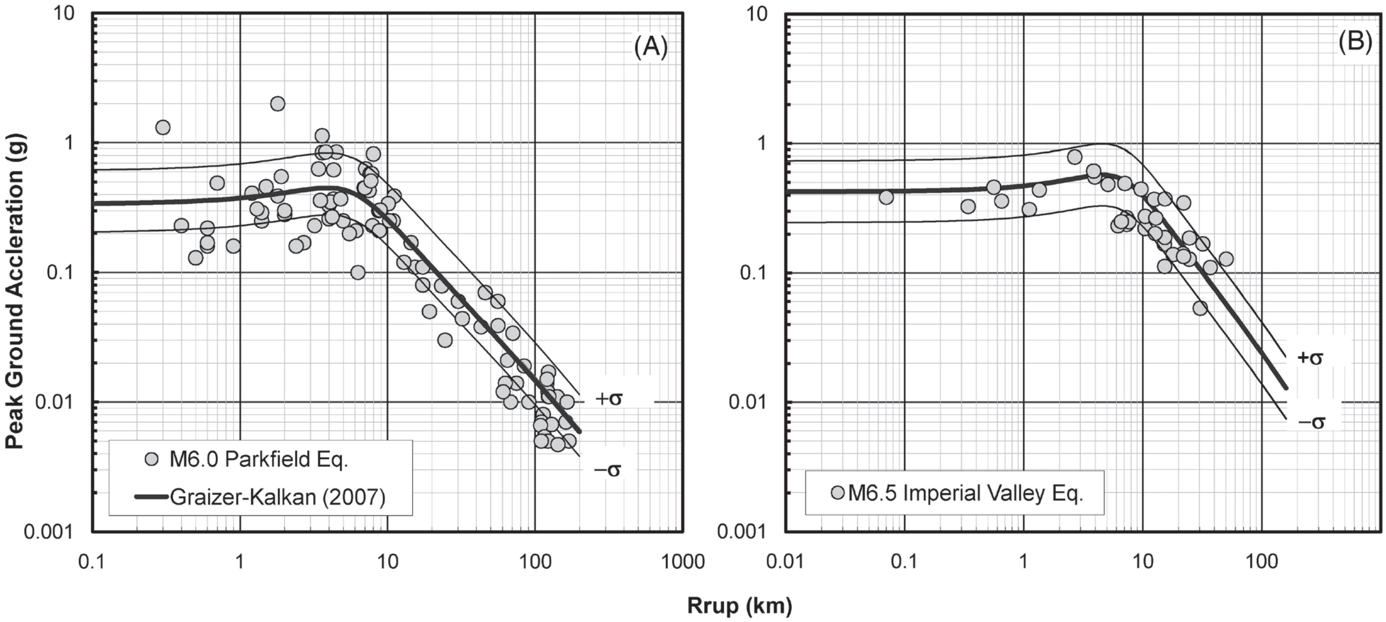

▲ **Figure 1.** Strong-motion data recorded during (A) 2004 **M** 6.0 Parkfield and (B) 1979 **M** 6.5 Imperial Valley earthquakes compared to predictions at 16, 50, and 84 percentile.

the size of the earthquake. Campbell (1981) suggested an idea similar to the corner distance in our model where he stated that "the distance at which transition from far-field to near-field attenuation occurs is deemed to be proportional to the size of the fault rupture zone, especially fault length for the larger shallow-focus event." Parameter D_0 is the damping term and describes the amplitude of the bump. Setting up damping to $D_0 = 0.7$ results in the absence of bump.

The amplitudes of PGA predicted for the Parkfield and Imperial Valley events are shown in Figure 1 at 16, 50, and 84 percentiles. The fact that the highest PGA was not recorded at the closest distance but at some distance from the fault was previously observed and discussed in the 1979 Imperial Valley earthquake dataset (N. Abrahamson, personal communication; see also Figure 10 in Campbell 1981). In an idealized case of uniform distribution of slip along the fault rupture, maximum ground motion occurs on the fault. However, if the fault-slip is not uniformly distributed and the fault itself is nonplanar, then the highest ground motion can be observed near the strongest asperity, with other near-field points having lower amplitudes. In this case, points at some distance from the fault plane (closest to lower amplitude of fault slip) can experience higher amplitude motion due to the effect of farther but stronger asperity, rather than the nearest point on the fault.

MODULAR FILTER-BASED APPROACH

We suggest using the following mathematical formulation instead of Equation 8 to represent ground motion attenuation.

$$PGA = G_1(M,F)\cdot G_2(M,R,C_2)\cdot G_3(M,R,C_3)\cdot G_4(M,C_4)\cdot G_5(M,R,C_5)\cdot \sigma_Y \tag{11}$$

In this representation, each function (G_n) is in multiplication form (that is, cascade of filters), helping to better understand its influence on the resultant ground-motion intensity measure. Equation 11 may be expressed in logarithmic space as:

$$\ln(PGA) = \sum_n \ln[G_n(M,R,C_n,F)] + \sigma_{\ln Y}\,. \tag{12}$$

Equation 12 is similar to the equation of a finite impulse response (FIR) filter, a digital filter characterized by its transfer function. Mathematical analysis of the transfer function can describe how it will respond to any input. For example, designing a filter consists of developing specifications appropriate to the problem and then producing a transfer function meeting these specifications. We suggest using a similar approach by creating an attenuation relation (transfer function) as a combination of filters, as shown in Equation 11. Analogous to the traditional seismological approach (*e.g.*, Boore 2003), the total spectrum of the motion at a site $Y(M_0,R,f)$ is split into four parts with contributions from earthquake source (E), path (P), site (G), and instrument or type of motion (I) as:

$$Y(M_0,R,f) = E(M_0,f)\cdot P(R,f)\cdot G(f)\cdot I(f) \tag{13}$$

where M_0 is the seismic moment.

Using separate functions (G_n) in series and modeling ground motion attenuation by means of an SDF response function provides the following advantages:

1. It allows representing each physical phenomenon on seismic radiation by a separate filter as a function of independent physical parameters (*e.g.*, M, R). This brings more physical meaning to each filter and consequently more connection to theoretical seismology.

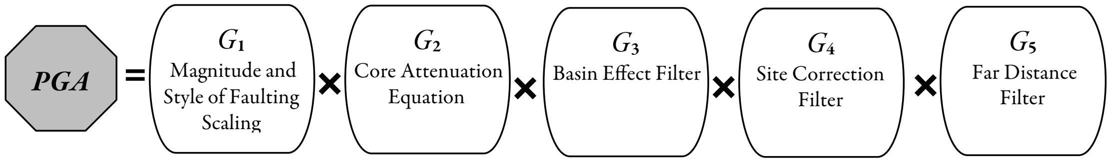

$$\ln(PGA) = \ln(G_1) + \ln(G_2) + \ln(G_3) + \ln(G_4) + \ln(G_5) + \sigma_{\ln(PGA)}$$

Modules

$$\ln(G_1) = \ln([c_1 \arctan(M + c_2) + c_3]F)$$
$$\ln(G_2) = -0.5\ln[(1 - r_2)^2 + 4D_2^2 r_2]$$
$$\ln(G_3) = -0.5\ln[(1 - \sqrt{r_3})^2 + 4D_3^2 \sqrt{r_3}]$$
$$\ln(G_4) = b_v \ln(V_{S30}/VA)$$
$$\ln(G_5) = c_{10} - 0.5\ln\left[(1 - \sqrt{R/R_5})^2 + 4D_5^2 \sqrt{R/R_5}\right]$$

where

$$r_2 = R/R_2$$
$$R_2 = c_4 M + c_5 \qquad D_2 = c_6 \cos[c_7(M + c_8)] + c_9$$
$$r_3 = R/R_3 \qquad R_3 = 100 \qquad D_3 = \begin{cases} 0.65 \text{ for } Z < 1 \text{ km} \\ 0.35 \text{ for } Z \geq 1 \text{ km} \end{cases}$$
$$R_5 = c_{11}M^2 + c_{12}M + c_{13}$$

Estimator Coefficients

c_1	c_2	c_3	c_4	c_5	c_6	c_7	c_8	c_9
0.14	-6.25	0.37	2.237	−7.542	-0.125	1.19	-6.15	0.525

c_{10}	c_{11}	c_{12}	c_{13}	D_5	b_v	VA	R_3
−0.16	18.04	−167.9	476.3	0.7	−0.24	484.5	100

Note **(1):** To capture basin effect it is recommended to set $D_3 = 0.35$, otherwise $D_3 = 0.65$
(2): $F = 1.00$ for strike-slip and normal faulting; $F = 1.28$ for reverse faulting
(3): R = Closest fault distance and M = Moment magnitude

▲ **Figure 2.** Graizer-Kalkan PGA attenuation relation for free-field maximum horizontal component of ground motion (Graizer and Kalkan 2007).

2. Instead of fitting an empirical equation to an entire database via single- or two-stage regression, the filter-based approach allows for sequential data fitting via robust nonlinear optimization (see for example, Graizer and Kalkan 2007).
3. It eliminates the need to search for a complex and purely empirical attenuation model that fits all distances.

Let us look at the filters used in our ground-motion attenuation model, developed for the range of magnitudes $5 < M < 8$ and distances up to 250 km. As shown in Figure 2, the first filter, G_1, is for magnitude and style of faulting scaling. The second filter, G_2, (called "core attenuation equation") models the attenuation of ground motion in the near-field. G_3 represents intermediate distance correction and basin effects. G_4 is for ground-motion amplification due to shallow site conditions, and G_5 adjusts the slope of the attenuation curve at far distances. Separate filters can represent amplification of ground motion at intermediate distances due to reflections from the Moho surface, near-field directivity, and hanging wall effects. Each filter utilized in our model is briefly explained as follows.

Filter G_1: Magnitude and Style of Faulting Scaling

The following scaling function models magnitude and style of faulting scaling:

$$A(M,F) = [c_1 \arctan(M + c_2) + c_3]\ F \tag{14}$$

where c_1, c_2, and c_3 are estimator coefficients and F represents scaling due to style of faulting. This scaling function reflects saturation of PGA with increasing moment magnitudes. According to the results of Sadigh *et al.* (1997), reverse fault events create ground motions approximately 28% higher than

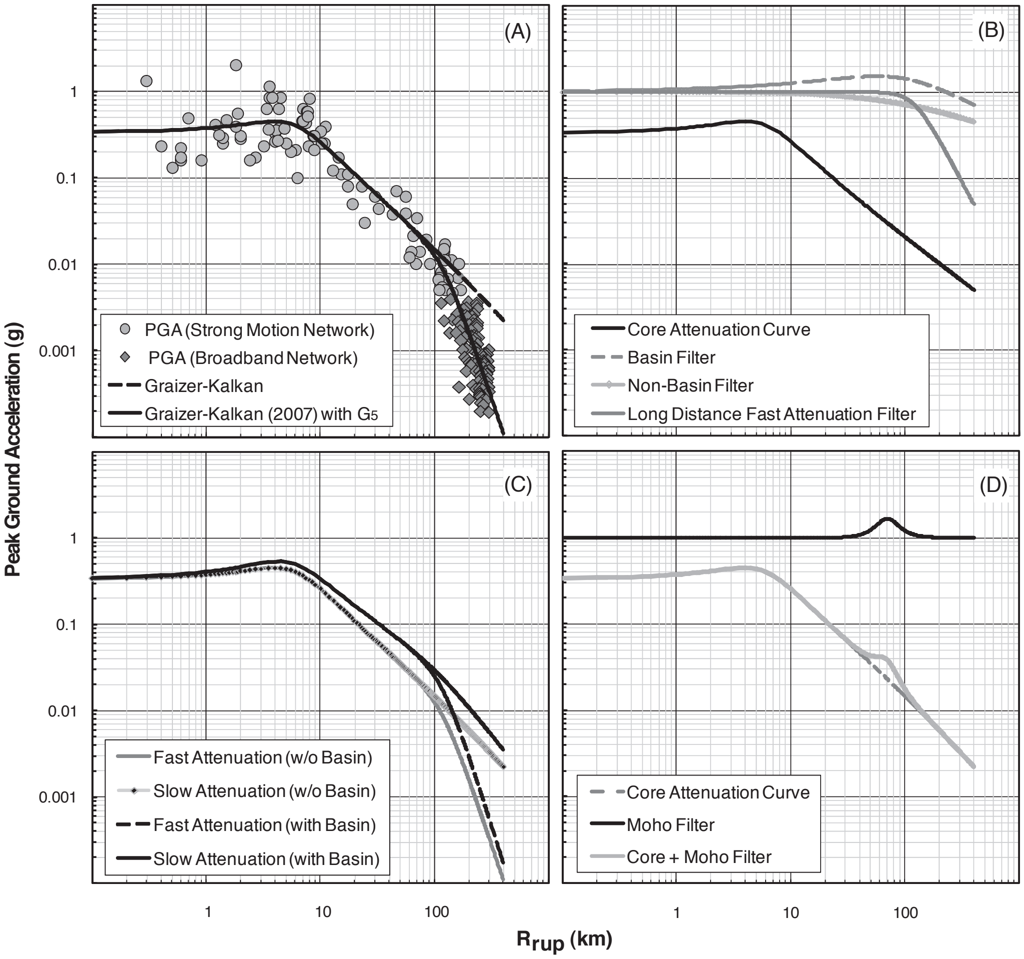

▲ **Figure 3.** A) 2004 **M** 6.0 Parkfield earthquake PGA data and approximation curves for ground-motion attenuation (low amplitude data shows faster attenuation); B) examples of filters modeling different physical phenomena including core attenuation, basin, and far distance fast attenuation; C) effects of basin filter and far distance fast attenuation filter on attenuation curve; D) modeling Moho reflection.

those from crustal strike-slips. Following this, we used $F = 1$ for strike-slip and normal faults and $F = 1.28$ for reverse faults.

Filter G_2: Core Attenuation Equation

In our model, the corner distance and damping in the core equation were denoted as R_0 and D_0. For consistency with G_2 in Equation 11 we refer to them as R_2 and D_2 in Equation 15. R_2 is a function of M, and D_2 quantifies the intensity of bump on the attenuation curve,

$$G_2(M,R,C_2) = 1 \Big/ \sqrt{\left[1-(R/R_2)\right]^2 + 4D_2^2(R/R_2)} \tag{15}$$

$$\begin{aligned} R_2 &= c_4 M + c_5 \\ D_2 &= c_6 \cos(c_7 M + c_8) + c_9 \end{aligned} \tag{16}$$

where c_4 and c_5 are estimator coefficients. Equations 15 and 16 imply that for larger magnitudes, the turning point on the attenuation curve occurs at larger distances. D_2 is a function of magnitude, reaching its minimum with $D_2 = 0.4$ (producing a significant bump) for **M** 6–6.5 and being higher at **M** < 5 and **M** > 7 (much lower or no bump), where c_6, c_7, c_8, and c_9 are estimator coefficients. The relative level of bump on the attenuation curve decreases at larger and smaller magnitudes. Recorded data show that the bump saturates at **M** > 7.5.

Filter G_3: Basin (Deep Sediment) Effect

Existence of deep sediments may amplify surface waves at distances more than 30 to 50 km (Lee *et al.* 1995; Campbell 1997; Frankel *et al.* 2001). We model this effect by applying the G_3 filter as shown in Figures 2 and 3. The G_3 filter has two parameters: Distance, R_3, and damping, D_3. R_3 describes the distance at which amplification (bump on attenuation curve) due to basin effect takes place and D_3 describes its amplitude (lower value of D_3 produces higher amplitudes of bump, see Figure 3B). If the sediment thickness is small, the basin effect can be neglected and D_3 can be taken as 0.65–0.7 (no bump). G_3 filter with this value of D_3 results in a change of slope of the attenuation curve at distances larger than R_3 only, and G_3 remains ineffective for distances less than R_3 (Figure 3B and C). R_3 is fixed to 100 km. Resultant attenuation function $(G_2 \cdot G_3)$

decays proportionally to $R^{-1.5}$ at distances $R > R_3$, unlike R^{-1} decay produced by the G_2 filter (Figure 3C).

We envision the damping parameter of the third filter (D_3) to be a smooth function of basin depth (thickness of sediment layer). As a first approximation, we considered the basin effect to be identical for all sediment depths (Z) more than 1 km (Graizer and Kalkan 2007; Graizer *et al.* 2010):

$$G_3(M,R,C_3) = 1 \Big/ \sqrt{\left[1-(R/R_3)^{0.5}\right]^2 + 4D_3^2(R/R_3)^{0.5}}$$

$$D_3 = \begin{cases} 0.65 \text{ for } Z < 1 \text{ km} \\ 0.35 \text{ for } Z \geq 1 \text{ km} \end{cases} . \tag{17}$$

D_3 is expected to decrease smoothly from 0.7 to 0.3–0.4 and saturate with an increase in sediment thickness.

Filter G_4: Effect of Shallow Site Conditions

Cross-comparison of the NGA relations demonstrates significant differences in site amplification for PGA and spectral acceleration ordinates for soft soils ($V_{S30} < 400$ m/s) (Idriss 2009). These differences call for further calibration of nonlinear models based on experimental data. On the basis of available studies (a list of references is given in Graizer and Kalkan 2007), we adopted a linear site amplification filter as

$$F_{site} = b_v \cdot ln(V_{S30}/V_A) \quad . \tag{18}$$

Equation 18 is the equivalent form of the linear site correction expression provided by Boore *et al.* (1997). In the linear site amplification formula of Boore *et al.*, $b_v = -0.371$, whereas our estimates yield $b_v = -0.24$. Similar to the findings of Field (2000), Equation18 with its parameters given in Figure 2 exhibits less amplification as the V_{S30} decreases compared to Boore *et al.* 1997.

Filter G_5: Far-Distance Attenuation Filter

The USGS Atlas global database, with 13,992 PGA data points from worldwide shallow crustal events (http://earthquake.usgs.gov/eqcenter/shakemap/atlas.php), indicates that ground-motion attenuation for distances more than 100 km has two main tendencies: faster attenuation in the order of R^{-4} and slower attenuation in the order of $R^{-1.5}$ (Graizer *et al.* 2010). Increase in the attenuation rate (that is, faster attenuation) is due to relatively low Q-values while decrease in the attenuation rate is due to high Q-values. For regions similar to the CEUS with relatively high Q-values (Singh and Herrmann 1983; Mitchell and Hwang 1987; Chandler *et al.* 2006), the attenuation rate at far-field is about the same as in near-field (about $R^{-1.5}$). In the WUS with relatively low Q-values, attenuation is faster (almost R^{-4}) at far distances. For example, the 2004 Parkfield earthquake exhibits faster ground-motion attenuation (Figure 3A) at distances >100 km. To model fast attenuation at far distances, the following filter can be implemented:

$$G_5(M,R_{cl}) = 1 \Big/ \sqrt{\left[1-(R/R_5)^d\right]^2 + 4D_5^2(R/R_5)^d} \tag{19}$$

G_5 has a flat region at distances $R < R_5$ and a turning point around the corner distance, R_5, for damping parameter, $D_5 = 0.6-0.7$. The rate of attenuation curve is determined by an adjustable parameter d, varying from 0 to 2.5; 0 means no adjustment to attenuation rate. In Equation 19, $R_5 = c_{11}M^2 + c_{12}M + c_{13}$. Corner distance R_5 increases with M. Use of G_5 with $d = 0.5$ brings the attenuation rate at far distances to $R^{-2.0}$. The G_5 filter practically does not affect distances closer to the fault than the corresponding corner distance (see Figure 3A and B). It allows for relatively fast change of rate, which is practically impossible in the classical approach using Equation 8.

The path effects on strong ground motion due to crustal structures have been known for a while. In central California, Bakun and Joyner (1984) suggested that the large positive residuals in M_L at distances between 75 and 125 km could be due to Moho reflections. Burger *et al.* (1987) showed that the observed interval of relatively high amplitudes in the distance range of 60 to 150 km in North America can be attributed to post-critically reflected S waves from the Moho discontinuity. Somerville and Yoshimura (1990) present evidence of enhanced amplitudes of strong ground motion from the 1989 Loma Prieta earthquake recorded at San Francisco and Oakland. Liu and Tsai (2009) showed the significant effect of Moho reflection on peak ground motion in northwestern Taiwan. With the methodology implemented herein, it is possible to add another filter to represent the Moho reflection as $G_6(M, R, C_6)$ (Figure 3D). We leave the calibration of this filter based on the recorded data for a future study.

PGA-BASED PREDICTIVE MODEL FOR SPECTRAL ACCELERATION

Our spectral acceleration (SA) prediction model for 5% damping explicitly integrates PGA as a scaling factor for the spectral shape, which is a continuous function of spectral period (or frequency). We used an empirical approach and found out that the summation of a modified lognormal probability density function $[F_1(T)]$ with an altered SDF oscillator transfer function $[F_2(T)]$ provided the desired shape and also enough flexibility to fit into a wide range of spectral shapes of earthquake recordings. Each one of these functions simulates certain spectral behavior; for that reason their unification $[F(T) = F_1(T) + F_2(T)]$ results in a desired predictive model. Thus, the model allows for prediction of SA at any period of interest within the model range of 0.01 to 10 s or even longer periods. Figure 4 summarizes the Graizer and Kalkan (2009) model. In this model, ζ controls the slope of spectral shape decay at long periods, with $\zeta = 1.5$ demonstrating best match to recorded data. The average spectrum has different decay before and after its predominant (peak) period; this peak period is identified by $\mu(M,R,V_{S30})$ and $T_{sp,0}(M,R,V_{S30})$. The wide-

$$\mathrm{SA}(T) = \mathbf{PGA} \times \left[SA_{\text{norm}}(T/M,R,V_{S30}) \right]$$

R = Closest fault distance
M = Moment magnitude

$$SA_{\text{norm}}(T/M,R,V_{S30}) = I(M,R)\,e^{-\frac{1}{2}\left(\frac{\ln(T)+\mu(M,R,V_{S30})}{S(M,R)}\right)^2} + \left[\left(1-\left(T/T_{sp,0}\right)^{\zeta}\right)^2 + 4D_{sp}^2\left(T/T_{sp,0}\right)^{\zeta}\right]^{-1/2}$$

$$\mu(M,R,V_{S30}) = m_1 R + m_2 M + m_3 V_{S30} + m_4$$
$$I(M,R) = (a_1 M + a_2)e^{a_3 R}$$
$$S(M,R) = s_1 R - (s_2 M + s_3)$$
$$T_{sp,0}(M,R,V_{S30}) = t_1 R + t_2 M + t_3 V_{S30} + t_4$$

m_1	m_2	m_3	m_4	a_1	a_2	a_3	D_{sp}
–0.0012	–0.4087	0.0006	3.63	0.017	1.27	0.0001	0.75

t_1	t_2	t_3	t_4	s_1	s_2	s_3	ζ
0.0022	0.63	-0.0005	-2.1	0.001	0.077	0.3251	1.5

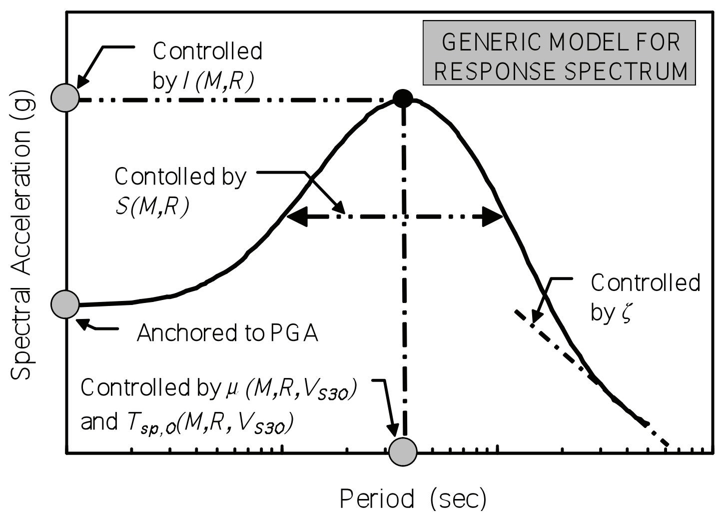

▲ **Figure 4.** PGA-based prediction model for 5% percent damped response spectral acceleration ordinates (Graizer and Kalkan 2009).

ness of the bell-shape of the spectrum is identified by $S(M, R)$ and D_{sp}. Parameters of the SA model shown in Figure 4 were computed through nonlinear optimization. The standard deviation of our SA model ranges from 0.544 at 0.01 s to 0.781 at 5 s (Table 2 in Graizer and Kalkan 2009), which is comparable to the recent NGA relations.

MODEL INPUT PARAMETERS

The number of input parameters in recent ground-motion attenuation relations (*e.g.*, Abrahamson and Silva 2008, Campbell and Bozorgnia 2008, Chiou and Youngs 2008) is much more than that from their respective earlier versions (Abrahamson and Silva 1997, Campbell 1997, Sadigh *et al.*, 1997). This trend is driven by an attempt to increase accuracy and efficiency in predictions. In the following, we categorize the parameters used in recent attenuation relations as primary and secondary:

Primary parameters:
1. Magnitude
2. Distance
3. Style of faulting
4. Site conditions: shallow site and deep sediment effects

Secondary parameters:
1. Hanging/foot wall effect
2. Depth to the surface of the rupture
3. Directivity effect
4. Earthquake source fault plane solution parameters (dip and rake angle)

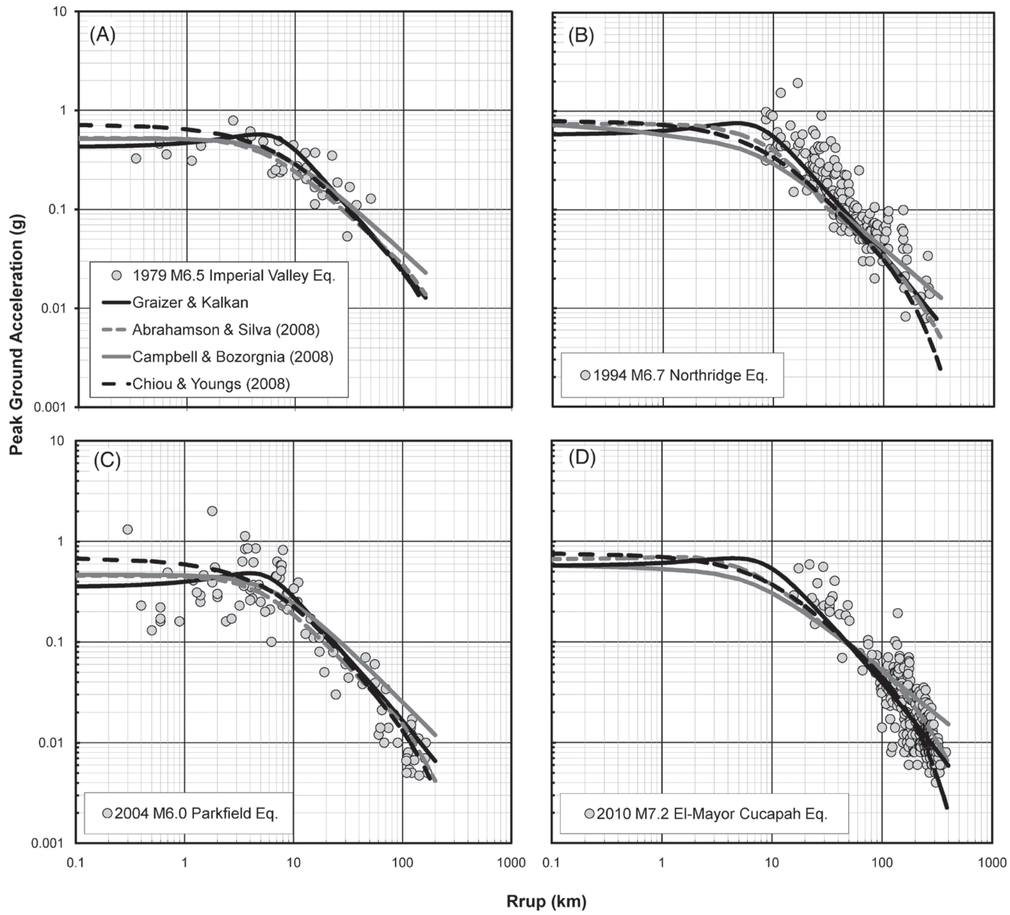

▲ **Figure 5.** Event-based comparisons of Graizer-Kalkan predictions with the NGA relations.

Abrahamson and Silva (2008), Campbell and Bozorgnia (2008), and Chiou and Youngs (2008) use all these input parameters except for directivity. Boore and Atkinson (2008) use the first set of input parameters without basin effect, and Idriss (2008) uses the first three parameters and a generalized site correction term for "deep or stiff soil." In our attenuation model, we only use the primary parameters, which are relatively easy to determine. The inclusion of secondary parameters results in significant complexity in the models. First, it requires above-average seismological training for users (not necessary available to all users), and second, these parameters are often non-unique. For example, for the San Simeon earthquake, the depth to the surface of the fault rupture and fault plane solution parameters vary significantly in different publications. These parameters might not be available immediately after the event.

COMPARISONS WITH NGA RELATIONS

To demonstrate the performance of the Graizer and Kalkan (2007) model, we first compare its predictions with recorded PGA data and three NGA relations (Abrahamson and Silva 2008, Campbell and Bozorgnia 2008, and Chiou and Youngs 2008) in Figure 5. The model of Boore and Atkinson (2008) is not included because of the different distance metric used. In comparison, we considered a number of relatively well-recorded events in California including the 1979 **M** 6.5 Imperial Valley, 1994 **M** 6.7 Northridge, 2004 **M** 6.0 Parkfield, and 2010 **M** 7.2 El Mayor–Cucapah earthquakes. All predictions are based on an average *S*-wave velocity of 400 m/s. Predictions by the three NGA relations for PGA are multiplied by a factor of 1.12 to convert their predictions from the geometric mean horizontal component to the maximum of the two as-recorded horizontal components; this adjustment factor was taken from Campbell and Bozorgnia (2007). Visual comparison of the predictions of our model with those of the three NGA relations shows that our predictions are in good agreement with the recorded data as well as with the predictions of the three NGA relations for a range of magnitudes and distances. In general, our predictions are higher, in the distance range of 5–10 km, than those from the three NGA relations. Between 20 and 100 km, our predictions and those of Abrahamson and Silva (2008) and Chiou and Youngs (2008) are almost identical.

Figure 6 compares the spectral acceleration predictions between our model and the four NGA relations (including Boore and Atkinson 2008, because at large fault distances the differences in distance metrics for these events is not significant) considering an average of 20 response spectra from the **M** 7.1 Hector Mine and the **M** 7.2 El Mayor–Cucapah earthquakes at the distance of approximately 190 km (with 10 average SA functions from each earthquake). Both earthquakes are similar in terms

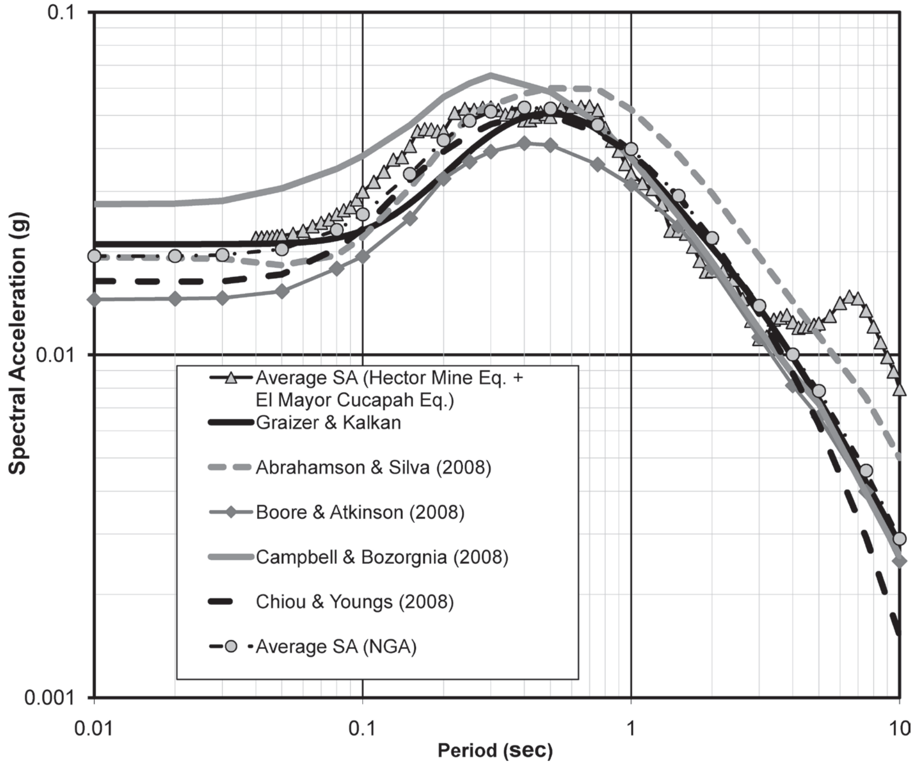

▲ **Figure 6.** Comparison of the average SA observed at the distance of approximately 190 km for the **M** 7.1–7.2 events with Graizer-Kalkan and NGA relations.

of magnitude and style of faulting (that is, strike slip), but the El Mayor–Cucapah earthquake (with magnitude slightly higher than that of the Hector Mine earthquake) produced almost two times lower average SA than that of the Hector Mine. The average response spectrum of the four NGA relations is almost the same as our predictions at periods longer than 0.5 s. At very short periods (0.01–0.05 s), our predictions are slightly higher than that of the average NGA curve and closer to the average recorded PGA. From 0.06 to 0.3 s, the average response spectrum of the four NGA relations is closer to the recorded data. The same plot also shows significant differences at long periods due to the basin effect in Los Angeles. All models, except Boore and Atkinson (2008), factor in basin effect yet tend to underestimate the spectral amplitudes at long periods (4 to 10 s). The difference is less for the Abrahamson and Silva relation at long periods. However, the Abrahamson and Silva model overpredicts at periods between 0.3 to 4 s. This plot demonstrates that our SA prediction model is in good agreement with the actual data and also with predictions from the three NGA relations.

CONCLUDING REMARKS

An attenuation relation is a mathematical representation of ground-motion signal transformation, due to numerous physical processes, from the earthquake source to a site. We found that a single-degree-of-freedom transfer function approximation, with a combination of filters, is an accurate (that is, providing expected median prediction) and efficient (that is, providing relatively small standard error of prediction) way to model this complex transformation. In a sense, it is analogous to the classical approach where the total spectrum of motion at a site is split into different parts with contributions from earthquake source, path, site, and instrument or type of motion. This approach also allows for relatively fast change of attenuation rate leading to better representation of regional variation in ground-motion prediction. In contrast to other models, our PGA-based predictive model for spectral acceleration is a continuous function of spectral period. Formulation of response spectrum by a continuous function of period allows calculation of its ordinates at any period of interest within the model range of 0.01 to 10 s and possibly beyond it. As shown here and in a number of other publications, the Graizer and Kalkan attenuation relation demonstrates good agreement with recorded data from past earthquakes as well as with the NGA relations.

DATA AND RESOURCES

The Graizer-Kalkan ground-motion prediction models for PGA and SA are available from the authors in Fortran, M.S. Excel, and MatLAB platforms.

ACKNOWLEDGMENTS

We wish to thank David Boore for providing us his Fortran code for NGA relations. Special thanks are extended to Rasool Anooshehpoor, Jon Ake, and an anonymous reviewer for reviewing this article and providing their valuable suggestions, which helped to improve its technical quality.

DISCLAIMER

Any opinions, findings, and conclusions expressed in this article are those of the authors and do not necessarily reflect the views of the United States Nuclear Regulatory Commission.

REFERENCES

Abrahamson, N. A., and W. J. Silva (1997). Empirical response spectral attenuation relations for shallow crustal earthquakes. *Seismological Research Letters* **68**, 94–127.

Abrahamson, N. A. and W. J. Silva (2008). Summary of the Abrahamson and Silva NGA ground motion relations. *Earthquake Spectra* **24** (1), 67–98.

Ambraseys, N. N. (1975). Trends in engineering seismology in Europe. *Proceedings of Fifth European Conference on Earthquake Engineering* **3**, 39–52.

Bakun, W. H., and W. B. Joyner (1984). The M_L scale in Central California. *Bulletin of the Seismological Society of America* **74**, 1,827–1,843.

Bolt, B. A., and N. A. Abrahamson (1982). New attenuation relations for peak and expected accelerations of strong ground motion. *Bulletin of the Seismological Society of America* **72**, 2,307–2,321.

Boore, D. M. (2003). Simulation of ground motion using the stochastic method. *Pure and Applied Geophysics* **160**, 635–676.

Boore, D. M., and G. M. Atkinson (2008). Ground motion prediction equations for the average horizontal component of PGA, PGV, and 5%-damped PSA at spectral periods between 0.01 s and 10.0 s. *Earthquake Spectra* **24** (1), 99–138.

Boore, D. M., W. B. Joyner, and T. E. Fumal (1997). Equations for estimating horizontal response spectra and peak acceleration from western North American earthquakes: A summary of recent work. *Seismological Research Letters* **68**, 128–153.

Brune, J. (1970). Tectonic stress and the spectra of seismic shear waves from earthquakes. *Journal of Geophysical Research* **75**, 4,997–5,009.

Brune, J. (1971). Correction. *Journal of Geophysical Research* **76**, 5,002.

Burger, R. W., P. G. Somerville, J. S. Barker, R. B. Herrmann, and D. V. Helmberger (1987). The effect of crustal structure on strong ground motion attenuation relations in eastern North America. *Bulletin of the Seismological Society of America* **77**, 420–439.

Campbell, K. W. (1981). Near-source attenuation of peak horizontal acceleration. *Bulletin of the Seismological Society of America* **71**, 2,039–2,070.

Campbell, K. W. (1997). Empirical near-source attenuation relations for horizontal and vertical components of peak ground acceleration, peak ground velocity, and pseudo-absolute acceleration response spectra. *Seismological Research Letters* **68**, 154–179.

Campbell, K. W. (2003). Strong-motion attenuation relations. In *International Handbook of Earthquake and Engineering Seismology,* Part B, ed. W. H. K. Lee, H. Kanamori, P. C. Jennings, and C. Kisslinger, 1,003–1,012. Boston, MA: Academic Press.

Campbell, K. W., and Y. Bozorgnia (2007). Campbell-Bozorgnia NGA Ground Relations for the Geometric Mean Horizontal Component of Peak and Spectral Ground Motion Parameters. Report Pacific Earthquake Engineering Research (PEER) Center 2007/02, 240 pp.

Campbell, K. W., and Y. Bozorgnia (2008). NGA ground motion model for the geometric mean horizontal component of PGA, PGV, PGD and 5% damped linear elastic response spectra for periods ranging from 0.01 to 10 s. *Earthquake Spectra* **24** (1), 139–172.

Chandler, A. M., N. T. K. Lam, and H. H. Tsang (2006). Near-surface attenuation modelling based on rock shear-wave velocity profile. *Soil Dynamics and Earthquake Engineering* **26** (11), 1,004–1,014.

Chinnery, M. A. (1961). The deformation of the ground around surface faults. *Bulletin of the Seismological Society of America* **51**, 355–372.

Chiou, B., and R. Youngs (2008). An NGA model for the average horizontal component of peak ground motion and response spectra. *Earthquake Spectra* **24** (1), 173–216.

Donovan, N. C. (1973). A statistical evaluation of strong motion data including the February 9, 1971 San Fernando earthquake. *Proceedings of Fifth World Conference on Earthquake Engineering* **1**, 1,252–1,261. Rome: IAEE.

Douglas, J. (2001). A comprehensive worldwide summary of strong-motion attenuation relationships for peak ground acceleration and spectral ordinates (1969–2000). ESEE Report No. 01-1. January 2001. London: Imperial College of Science, Technology and Medicine, 144 pp.

Douglas, J. (2002). Errata of an additions to ESEE Report No. 01-1, "A comprehensive worldwide summary of strong-motion attenuation relationships for peak ground acceleration and spectral ordinates (1969–2000)." October 2002. London: Imperial College of Science, Technology and Medicine, 40 pp.

Esteva, L. (1970). Seismic risk and seismic design. In *Seismic Design for Nuclear Power Plants*, 142–182, ed. R. J. Hansen. Cambridge, MA: M.I.T. Press.

Esteva, L., and E. Rosenblueth (1964). Espectios de temblores a distancias moderadas y grandes. *Proceedings of the Society of Mexican Engineering Seismologists Chilean Conference on Seismology and Earthquake Engineering*, University of Chile.

Field, E. H. (2000). A modified ground motion attenuation relationship for Southern California that accounts for detailed site classification and a basin-depth effect. *Bulletin of the Seismological Society of America* **90**, 209–221.

Frankel, A., D. Carver, E. Cranswick, T. Bice, R. Sell, and S. Hanson (2001). Observation of basin ground motions from a dense seismic array in San Jose, California. *Bulletin of the Seismological Society of America* **91,** 1–12.

Graizer, V., and E. Kalkan (2007). Ground motion attenuation model for peak horizontal acceleration from shallow crustal earthquakes. *Earthquake Spectra* **23** (3), 585–613.

Graizer, V. and E. Kalkan (2009). Prediction of response spectral acceleration ordinates based on PGA attenuation. *Earthquake Spectra* **25** (1), 39–69.

Graizer, V., E. Kalkan, and K.W. Lin (2010). Extending and testing Graizer-Kalkan ground motion attenuation model based on Atlas database of shallow crustal events. *Proceedings of the 9th U.S. National and 10th Canadian Conference on Earthquake Engineering.* Toronto, Ontario, Canada, 25–29 July 2010. Paper no. 568, Earthquake Engineering Research Institute/Canadian Association for Earthquake Engineering (EERI/CAEE).

Haskell, N. A. (1969). Elastic displacements in the near-field of a propagating fault. *Bulletin of the Seismological Society of America* **59**, 865–908.

Idriss, I. M. (2008). An NGA empirical model for estimating the horizontal spectral values generated by shallow crustal earthquakes. *Earthquake Spectra* **24** (1), 217–242.

Idriss, I. M. 2009. Use of Vs30 to Represent Effects of Local Site Conditions on Earthquake Ground Motions (abstract). *Seismological Research Letters* **80** (2), 363.

Joyner, W. B., and D. M. Boore (1981). Peak horizontal acceleration and velocity from strong-motion records including records from the 1979 Imperial Valley, California, earthquake. *Bulletin of the Seismological Society of America* **71**, 2,011–2,038.

Lee, V. W., M. D. Trifunac, M. I. Todorovska, and E. I. Novikova (1995). *Empirical Equations Describing Attenuation of Peak of Strong Ground Motion, in Terms of Magnitude, Distance, Path Effects and Site Conditions*. Report No. CE 95-02. Los Angeles, California: Department of Civil Engineering, University of Southern California, 268 pp.

Liu, K. S., and Y. B. Tsai (2009). Large effects of Moho reflections (*SmS*) on peak ground motion in northwestern Taiwan. *Bulletin of the Seismological Society of America* **99**, 255–267.

Milne, W. G., and A. G. Davenport (1969). Distribution of earthquake risk in Canada. *Bulletin of the Seismological Society of America* **59**, 729–754.

Mitchell, B. J., and H. J. Hwang (1987). Effect of low *Q* sediments and crustal *Q* on *Lg* attenuation in the United States. *Bulletin of the Seismological Society of America* **77** (4), 1,197–1,210.

Power, M., B. Chiou, N. Abrahamson, and C. Roblee (2006). The next generation of ground motion attenuation models (NGA) project: An overview. In *Proceedings, Eighth National Conference on Earthquake Engineering*, paper No. 2022. San Francisco, California: Earthquake Engineering Research Institute (EERI).

Sadigh, K., C.-Y. Chang, J. A. Egan, F. Makdisi, and R. R. Youngs (1997). Attenuation relationships for shallow crustal earthquakes based on California strong motion data. *Seismological Research Letters* **68**, 180–189.

Schnabel, P. B., and H. B. Seed (1973). Accelerations in rock for earthquakes in the western United States. *Bulletin of the Seismological Society of America* **63**, 501–516.

Singh, S., and. R. B. Herrmann (1983). Regionalization of crustal coda *Q* in the continental United States. *Journal of Geophysical Research* **88**, 527–538.

Somerville, P. G., and J. Yoshimura (1990). The influence of critical Moho reflections on strong ground motions recorded in San Francisco and Oakland and during the 1989 Loma Prieta earthquake. *Geophysical Research Letters* **17**, 1,203–1,206.

Trifunac, M. D. (1976). Preliminary analysis of the peak of strong earthquake ground motion—dependence of peaks on earthquake magnitude, epicentral distance, and recording site conditions. *Bulletin of the Seismological Society of America* **66**, 189–219.

Trifunac, M. D., and A. G. Brady (1975). On the correlations of peak acceleration of strong motion with earthquake magnitude, epicentral distance and site conditions. In *Proceedings of the U.S. National Conference on Earthquake Engineering*, 43–52. Ann Arbor, MI: University of Michigan.

U.S. Nuclear Regulatory Commission
vladimir.graizer@nrc.gov
(V. G.)